

Full-Brain Coverage and High-Resolution Imaging Capabilities of Passband b-SSFP fMRI at 3T

Jin Hyung Lee,^{1*} Serge O. Dumoulin,² Emine U. Saritas,¹ Gary H. Glover,³ Brian A. Wandell,² Dwight G. Nishimura,¹ and John M. Pauly¹

Passband balanced-steady-state free precession (b-SSFP) fMRI is a recently developed method that utilizes the passband (flat portion) of the b-SSFP off-resonance response to measure MR signal changes elicited by changes in tissue oxygenation following increases in neuronal activity. Rapid refocusing and short readout durations of b-SSFP, combined with the relatively large flat portion of the b-SSFP off-resonance spectrum allows distortion-free full-brain coverage with only two acquisitions. This allows for high-resolution functional imaging, without the spatial distortion frequently encountered in conventional high-resolution functional images. Finally, the 3D imaging compatibility of the b-SSFP acquisitions permits isotropic-voxel-size high-resolution acquisitions. In this study we address some of the major technical issues involved in obtaining passband b-SSFP-based functional brain images with practical imaging parameters and demonstrate the advantages through breath-holding and visual field mapping experiments. Magn Reson Med 59:1099–1110, 2008. © 2008 Wiley-Liss, Inc.

Key words: SSFP; b-SSFP; fMRI; diffusion; oxygen; brain

Balanced-steady-state free precession (b-SSFP) imaging is an image acquisition technique that uses rapid RF excitation pulses combined with fully balanced gradient pulses during each excitation repetition interval (T_R) (1,2). Due to its short readout time and T_R , b-SSFP provides distortion-free 3D imaging suitable for full-brain, high-resolution functional imaging.

The first use of b-SSFP for functional MRI (fMRI) was proposed by Scheffler et al. (3), which used the steep magnitude transitional portion of the b-SSFP resonance spectrum to generate oxygen contrast based on the resonance frequency shift induced by deoxyhemoglobin. Another acquisition scheme using the steep phase transition of the b-SSFP off-resonance spectrum was subsequently proposed by Miller et al. (4) (Fig. 1b). We refer to these techniques as transition-band b-SSFP fMRI methods. Transition-band b-SSFP fMRI combines the advantages of b-SSFP imaging with a functional contrast mechanism sensitive to the deoxyhemoglobin frequency-shift following neuronal activations. In contrast, in conventional gradient-

echo (GRE) blood oxygenation level-dependent (BOLD) fMRI (5–7) using echo-planar imaging (EPI) with long echo time (T_E) and readout time, venous signal dephasing due to deoxygenation is both the source of functional signals, as well as the main source for signal dropouts and image distortions. Despite its potential for functional imaging, the use of the transition-band b-SSFP can be challenging. Transition-band b-SSFP methods produce oxygenation-sensitive contrast only in a very narrow range of frequencies near resonance. This requires the use of multi-frequency acquisitions even for a small volume coverage (8).

Here we describe an alternative approach, termed passband b-SSFP fMRI (9–14), which has the potential to provide distortion-free, high-spatial-resolution fMRI studies. The passband b-SSFP fMRI utilizes the flat portion of the b-SSFP off-resonance profile instead of the steep transitional portion (see Fig. 1c). Here the rapid refocusing of b-SSFP imaging suppresses larger scale off-resonance effects. This refocusing degrades when the off-resonance is spatially in the scale of the water diffusion distances (compare Fig. 1e,f). The resulting dephasing is expected to produce oxygenation contrast predominantly in parenchymal regions near small vessels with steep off-resonance changes. This mechanism is assumed to be similar to that of spin-echo (SE)-based fMRI. The difference in contrast mainly comes from the signal augmenting stimulated echo pathways that exist in b-SSFP acquisitions. Imaging constraints such as acquisition speed, distortion properties, and signal-to-noise ratio (SNR) add further advantages for passband b-SSFP-based fMRI. Bowen et al. (13,14) demonstrated passband b-SSFP fMRI's potential to sensitize itself to signal changes arising from the smaller vessel size of interest, while Lee et al. (9–11) proposed passband b-SSFP schemes combined with 3D imaging trajectories and multiple-acquisition techniques. The functional contrast mechanisms of passband b-SSFP techniques were investigated and compared to more conventional GRE-BOLD contrast by several groups through experimental and/or simulation studies (12,15–18).

In this article we demonstrate the applicability of passband b-SSFP for distortion-free, full-brain coverage and high spatial resolution isotropic functional imaging. The results of our studies suggest that distortion-free fMRI can be performed within neuroscientifically relevant temporal resolution and hardware constraints.

THEORY

While the detailed biophysics of passband b-SSFP functional signal source remains elusive, the most parsimonious explanation of the contrast mechanism for passband b-SSFP fMRI is the dephasing that is not refocused around

¹Magnetic Resonance Systems Research Laboratory, Department of Electrical Engineering, Stanford University, Stanford, California.

²Department of Psychology, Stanford University, Stanford, California.

³Radiological Sciences Laboratory, Department of Radiology, Stanford University, Stanford, California.

Grant sponsor: National Institutes of Health; Grant number: R01EB006471; Grant sponsor: GE Healthcare.

*Correspondence to: Jin Hyung Lee, 350 Serra Mall, #212, Stanford University, Stanford, CA 94305-9510. E-mail: ljinhy@stanford.edu

Received 3 August 2007; revised 16 December 2007; accepted 8 January 2008.

DOI 10.1002/mrm.21576

Published online 27 March 2008 in Wiley InterScience (www.interscience.wiley.com).

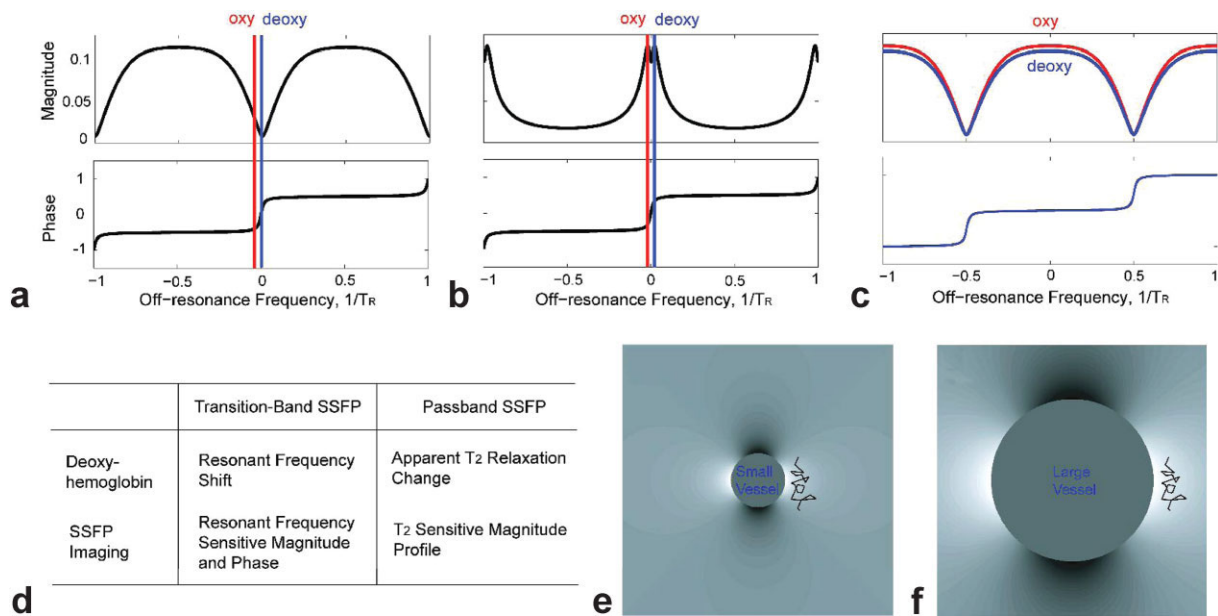


FIG. 1. b-SSFP fMRI methods. The two transition-band b-SSFP fMRI methods (**a,b**) depend on the sharp magnitude and phase transition of the b-SSFP off-resonance response while the passband b-SSFP fMRI method (**c**) utilizes the flat portion of the b-SSFP off-resonance profile. Differences between transition-band and passband b-SSFP properties are summarized in (**d**). **e**: The contrast is expected to be maximized near small vessels where water molecules experience rapid off-resonance frequency change during each T_R . **f**: For larger vessels water diffuses in a relatively uniform field during each T_R . The wiggly lines in (**e**) and (**f**) represent the typical water diffusion distances.

the off-resonance created by the deoxyhemoglobin (12,15,16,19,20). The rapid refocusing mechanism in b-SSFP imaging allows for the refocusing of any large-scale off-resonance effects. However, when the off-resonance effects are in the spatial scale of the water diffusion distance during T_R , the dephasing effects cannot be refocused (see Fig. 1e,f). This mechanism can be considered to be similar to that of SE-BOLD. The main difference relative to SE-BOLD is the fact that b-SSFP imaging allows for stimulated echo pathways that can in turn increase the overall signal and contrast. The flexibility in choosing the T_R also allows control over the diffusion distance of the water molecules in between the excitations. As evidenced by earlier studies, with this contrast mechanism passband b-SSFP fMRI has the potential to generate spatial scale selectivity (12,15,16,19,20). For voxels mostly containing small vessels, most of the dephasing effects are expected to come from the extravascular components. However, voxels containing large vessels will also produce signal from intravascular components. The intravascular component's b-SSFP signal dependency is mainly due to the diffusion of water molecules in and out of the red blood cells as described earlier (19). Another potential additional source for contrast in passband b-SSFP fMRI could originate from the hypothesized activity-dependent change in the diffusion of water molecules as proposed by Le Bihan et al. (21). With the possible decrease in diffusion during activation, the slower diffusion would further decrease dephasing during activation in addition to the effect due to the decrease in the deoxyhemoglobin concentration. The diffusion effects could therefore potentially further enhance the functional contrast in the extracellular space around the small vessels.

From the imaging perspective, passband b-SSFPs unique features make it well suited for distortion-free, high-resolution functional signal acquisitions. In passband b-SSFP fMRI the rapid excitation repetition intervals allow short segmented readouts that result in images with distortion levels similar to that of the T_1 -weighted anatomical acquisitions (compare sequences for GRE-BOLD and b-SSFP fMRI in Fig. 2a,b). Distortion-free, high-resolution acquisitions are important for brain function studies since gray matter voxels separated by only a few millimeters can have highly distinct functional properties (22,23). With conventional GRE-BOLD EPI acquisitions, a variety of methods have been proposed to reduce signal dropout and spatial distortions (24–27). While most of these methods are also compatible with b-SSFP acquisitions, the inherently distortion-free nature of the b-SSFP acquisition circumvents the aforementioned needs for improving distortion characteristics. In the presence of spatial distortions, even with high nominal encoding resolutions, the effective spatial resolution can also be greatly reduced. Neighboring voxels may not be accurately identified and assigned in the image space. Furthermore, spatial distortions limit the readout length, further constraining the acquisition resolution itself. Reduced distortion in conjunction with 3D acquisitions gives passband b-SSFP the potential for high-resolution functional images with isotropic voxels.

MATERIALS AND METHODS

Acquisition

For b-SSFP fMRI with adequate resolution and coverage, fast 3D acquisition techniques were combined with the

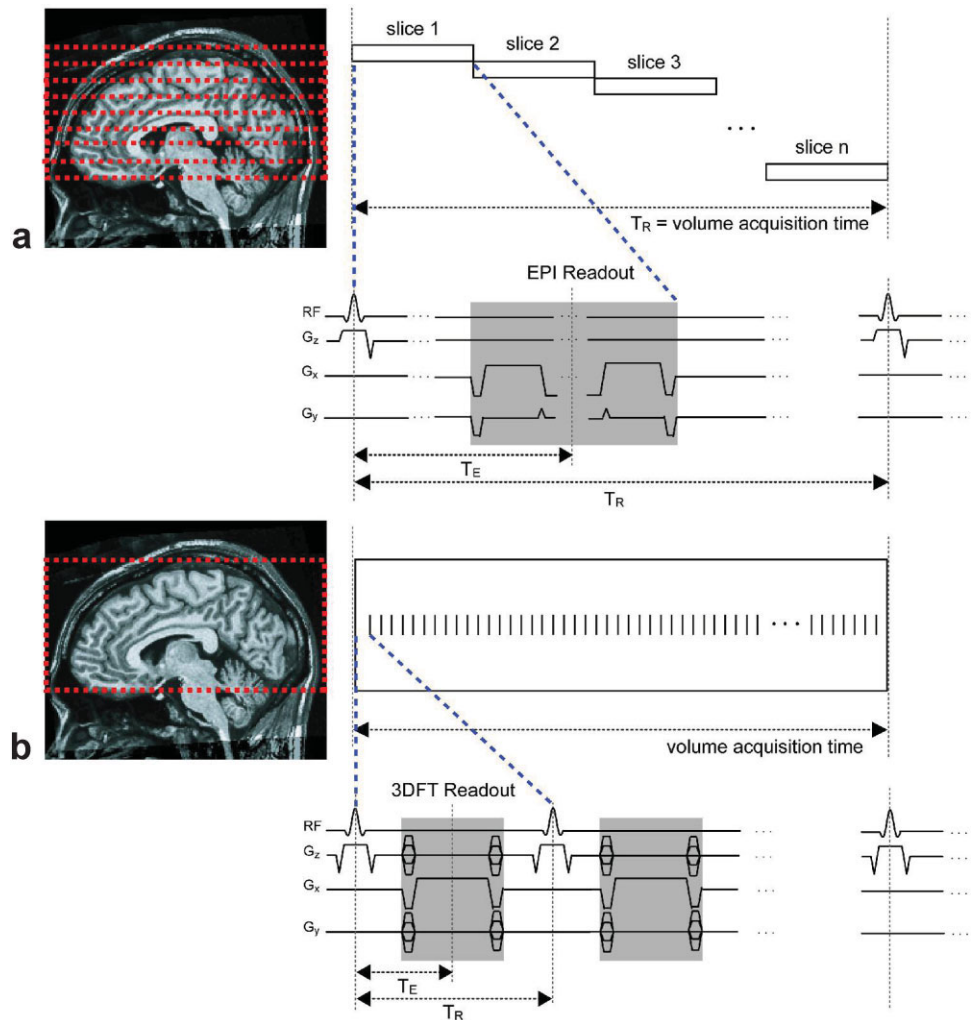


FIG. 2. Pulse sequences for GRE-BOLD and b-SSFP fMRI. The GRE-BOLD pulse sequences (a) involve long T_E and long T_R with interleaved multi-slice acquisitions while the b-SSFP fMRI pulse sequences (b) are volumetric multi-shot acquisitions with short T_E , short T_R , and fully balanced gradients for every T_R .

two-acquisition method (9,11) for whole-brain coverage. The corresponding SNR and specific absorption rate (SAR) were also calculated for comparison with the conventional methods.

3D Acquisition

b-SSFP acquisition involves short T_R , typically a few milliseconds to at most tens of milliseconds. Such short T_R allows 3D imaging compatibility. Furthermore, in the presence of blood flow and motion, 3D volumetric acquisitions provide a much more stable steady-state compared to the 2D acquisitions that will inevitably have blood flowing in and out of the thin slice while the location of the slice also changes with motion. 2D multi-slice acquisitions can also lead to additional overhead in scan time to move in and out of steady-state for each slice. Therefore, 3D volumetric acquisition is a natural choice to obtain proper contrast and efficient spatial coverage for b-SSFP fMRI acquisitions.

For 3D acquisitions the most straightforward strategy is to use 3D Cartesian (3DFT) trajectories (Fig. 3a). Because the T_R s are short, the acquisition time using 3DFT is feasible for a relatively low-resolution and small-volume coverage. However, to obtain high-resolution acquisitions

with practical volume coverage, an alternative acquisition strategy is necessary. To achieve such a goal, we chose interleaved stack-of-EPI and interleaved stack-of-spiral acquisitions (Fig. 3b,c).

To compare the efficiency of different acquisition strategies, scan times were compared in Fig. 3d,e. The comparison was performed for two different cases with different coverage and resolution (see legend to Fig. 3d,e for further details). The first case was for whole-brain coverage and the second case was for high-resolution acquisition of a small volume of interest. Scan time was calculated as a function of T_R . The choice of T_R can potentially determine the spatial scale sensitivity as well as the overall functional contrast. Therefore, the comparison is valid only for identical T_R s.

Two-Acquisition Method

Functional brain imaging studies often target a specific brain area such as the primary visual cortex. In such cases it is only necessary to image a localized region of the brain. To cover a certain localized region using passband b-SSFP fMRI methods, one simply needs to select the region of interest, shim around that region, and then perform the acquisition. To fine tune the volume of interest, phase-

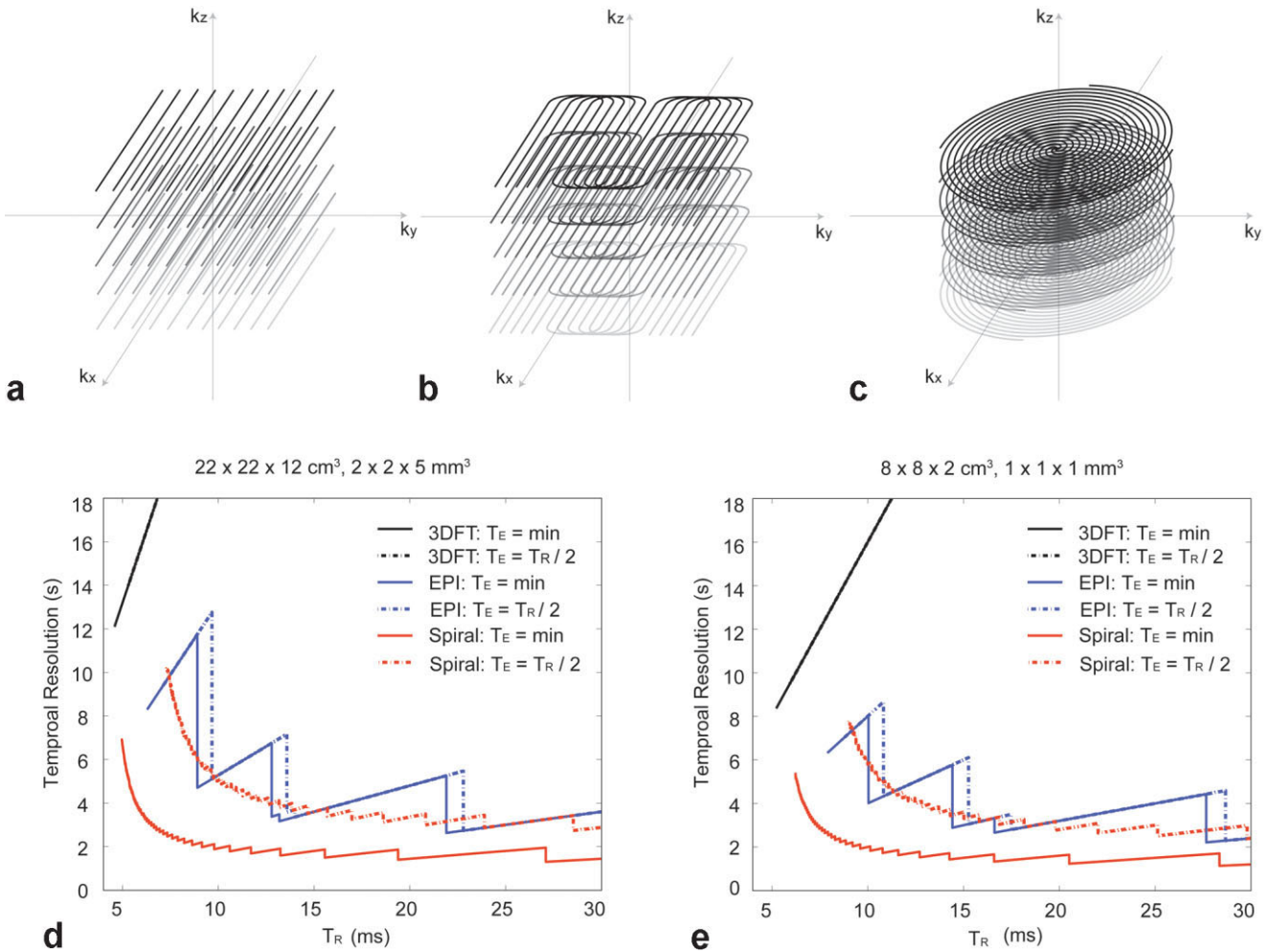


FIG. 3. 3D k -space trajectories and scan time for b-SSFP fMRI. **a**: Any 3D imaging trajectories can be incorporated into a b-SSFP acquisition including simple 3DFT readout. To allow fast acquisitions for high spatial and temporal resolution, stack-of-EPI (**b**) and stack-of-spirals (**c**) trajectories can be used. Scan time was calculated for different k -space sampling strategies for the whole brain imaging protocol (**d**) and the high-resolution imaging protocol (**e**). Since T_R is an important design parameter for spatial scale selectivity, scan time was calculated for a range of T_R s.

cycling angles can also be adjusted to shift the passband region of the b-SSFP response. Due to the relatively large volume coverage provided by the large flat portion of the b-SSFP off-resonance profile, a single acquisition is often sufficient for targeted region-of-interest (ROI) scans.

However, when whole-brain coverage is required, two acquisitions with different phase-cycling angles (28) can be combined (see Fig. 4). With two acquisitions at a 180° phase-cycling angle and a 0° phase-cycling angle, the entire off-resonance spectrum can be covered with the passband region of at least one of the two acquisitions (9,11,28). To avoid mixing contrast from the passband region and the transition-band region, a maximal intensity projection (MIP) method was chosen for the combination. The passband (flat) portion of the b-SSFP off-resonance spectrum has a higher signal level. Therefore, by selecting pixels from the images that have higher signal intensity, the passband acquired portion can be selected. The pixel selection was performed with the temporally averaged image from the whole fMRI acquisition so that each pixel is selected from one phase-cycling angle image throughout

the time series. The MIP selection was then low-pass filtered to generate a selection mask that has a more continuous region unaffected by noise.

It is important to note that while the two-acquisition method can cover the whole brain with just two acquisitions, in some cases it may not be possible to repeat two identical exams. For example, the novelty of stimuli may be crucial for the experimental design. To avoid such problems, alternating between the two steady-states can be a useful approach. However, there will be scan time overhead during the transition, which will limit the temporal resolution.

Signal-To-Noise Ratio

When imaging at the given field strength and RF coil, the SNR associated with thermal noise is proportional to the following parameters where $f(\rho, T_1, T_2)$ is the pulse sequence dependent function that determines the signal amplitude.

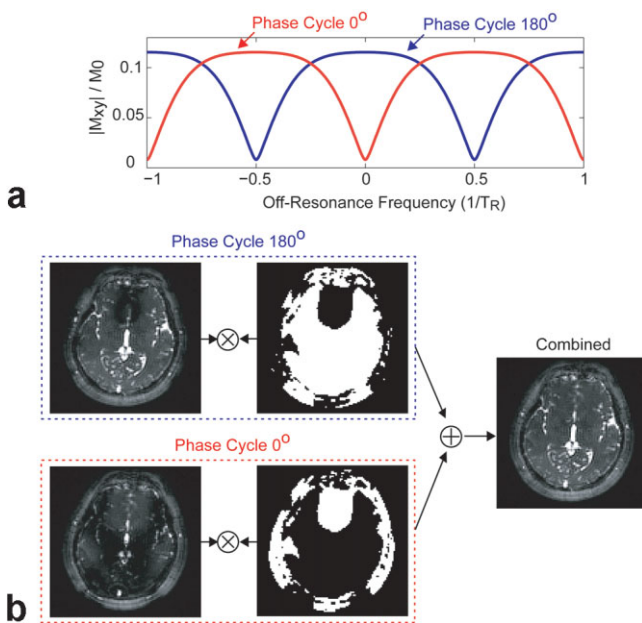


FIG. 4. Two-acquisition method for passband b-SSFP fMRI. **a:** By combining the 180° phase-cycled image and the 0° phase-cycled image, the passband of the two acquisitions cover the entire off-resonance spectrum. **b:** The two images are combined using MIP (instead of methods such as sum-of-squares) to select regions with pure passband contrast.

$$SNR \propto (\text{Voxel Size}) \times \sqrt{(\text{Total Readout Interval})} \times f(\rho, T_1, T_2) \quad [1]$$

For acquisitions with the same spatial and temporal resolution, the voxel size is constant while the total readout and the function f depend on the pulse sequence. The total readout interval is dependent on the readout duty cycle defined as the ratio of the readout time per each T_R . For GRE-BOLD imaging, the readout duty cycle is between 0.01 to 0.02 ($T_R = 1.5\text{--}3$ s, readout duration of 100 ms). Passband b-SSFP imaging has higher readout duty cycle in the range of 0.2–0.8 ($T_R = 5\text{--}20$ ms, readout duration of 2–16 ms). When T_R is kept constant, the signal intensity (f) is higher in the case of b-SSFP imaging compared to GRE. However, since typical functional acquisitions for GRE-BOLD involve longer T_R than that involved in b-SSFP imaging, f is usually larger in the case of GRE-BOLD. In the gray matter, f is typically 3–5 times larger in GRE-BOLD compared to b-SSFP imaging. Overall, the thermal noise SNR for passband b-SSFP is approximately 2–27 times higher than that of GRE-BOLD. This analysis is neglecting physiological noise. When the physiological noise is the dominant source of noise, such improvements in SNR will not be apparent. However, for high-resolution scans the thermal noise is expected to be an increasingly dominant source of noise. For example, for the $1 \times 1 \times 1$ mm³ resolution protocol described in the visual field mapping experiment, the expected b-SSFP acquisition SNR is 4.02 times larger compared to that of GRE-BOLD.

Specific Absorption Rate

SAR can be compared based on the RF energy deposition for each imaging method. Simple calculations can provide comparisons for GRE-BOLD, SE-BOLD, and b-SSFP fMRI methods.

For GRE-BOLD and SE-BOLD, imaging is typically done with the multi-slice acquisition scheme. With the multislice approach, while the T_R for each slice is long, the RF energy is deposited in the whole imaging volume every time an RF pulse is played out for each slice excitation. Therefore, the difference in RF energy deposition for GRE-BOLD, SE-BOLD, and passband b-SSFP fMRI methods can be calculated by calculating the difference in RF power deposition per T_R times the difference in number of interleaves used for the in-plane encoding. This is assuming the same number of slices is being encoded for all three methods.

As for the RF power deposition per T_R , GRE-BOLD typically uses 30–90° flip angles; SE-BOLD involves a 90° and a 180° pulse, while passband b-SSFP method can be used with a 30–60° flip angle pulse. Since the GRE or SE-BOLD acquisitions are usually performed in 1–2 shots, while the passband b-SSFP method requires 10–20 shots for each phase-encoding location, the difference is 5–20 times more RF pulses for passband b-SSFP methods. Overall, the SE-BOLD method has 5–45 times higher SAR compared to GRE-BOLD and the passband b-SSFP method has 0.56–80 times SAR compared to the GRE-BOLD method. The passband b-SSFP fMRI method has a number of parameters that can be quite flexibly selected so that a comparable SAR can be achieved as GRE-BOLD if needed. For example, in the case of the whole-brain coverage protocol used for the breath-holding experiments described below, compared to the GRE-BOLD, SAR of passband SSFP fMRI is only 1.54 times higher while the SAR of SE-BOLD is 8.27 times higher.

Functional MRI Studies

Several experiments were performed to demonstrate the viability and unique capabilities of passband b-SSFP based functional imaging (Fig. 5). All experiments were conducted using a GE 3 T Excite system with a maximum gradient amplitude of 40 mT/m and maximum slew rate of 150 T/m/s. A total of 15 normal healthy volunteers participated in the study with the approval of the Stanford University Institutional Review Board (13 males, 2 females; 23–55 years old). Subjects were individually recruited for a single session. Some subjects participated in more than one session but no subject participated in all the different types of studies. All the results presented in this study were obtained with spiral acquisitions for both the GRE-BOLD and passband b-SSFP fMRI studies. For all experiments, four dummy acquisitions were used. In the case of passband b-SSFP acquisitions, four dummy acquisitions, which included more than 1000 dummy T_{RS} , were used to make sure steady-state was reached before the actual fMRI scans. The flip angles for GRE-BOLD acquisitions were 70°, and for passband b-SSFP acquisitions 30° (other than for the hemodynamic response function measurements with varying flip angles). The GRE-BOLD acquisitions all had a T_E of 30 ms and the passband b-SSFP

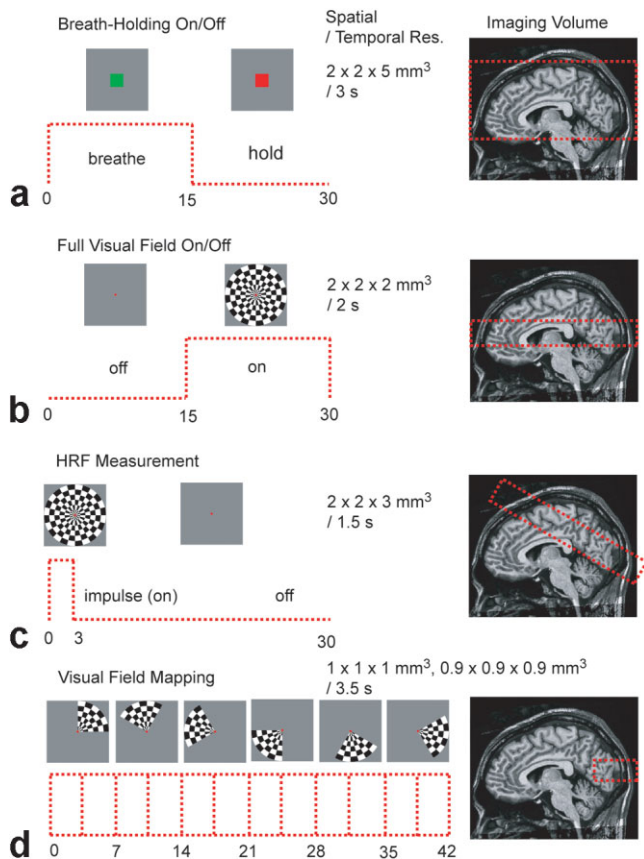


FIG. 5. Experiments conducted using passband b-SSFP fMRI.

acquisitions all had minimum T_E . The minimum T_E depends on the slice-select z-gradient rewinder duration and the z-phase encoding gradient duration. Therefore, the thinner the slab and the higher the z-resolution, the minimum T_E becomes longer except for the $0.9 \times 0.9 \times 0.9 \text{ mm}^3$ resolution retinotopy experiment where the minimum T_E was further reduced by combining the slice select gradient rewinder and the phase encode gradient. Figure 5 summarizes the different functional paradigms and the corresponding imaging volumes used for our experimental studies.

Breath-Holding Experiment

Breath-holding experiments were designed to demonstrate the capability of passband b-SSFP fMRI for distortion-free full-brain coverage. Hypercapnia induced by breath-holding increases cerebral blood flow (CBF), resulting in increased oxygenation across the entire brain (29). Breath-holding is thus a simple and robust method to elucidate the extent to which a particular functional imaging technique can measure the degree of oxygenation saturation across the whole brain. In this study, to compare the effectiveness of the full-brain coverage, breath-holding experiments were conducted with GRE-BOLD and passband b-SSFP fMRI in the same subjects within the same imaging session lasting for less than 30 min. The GRE-BOLD technique was chosen for comparisons since it is the most widely accepted method for functional brain imaging.

The GRE-BOLD and passband b-SSFP fMRI experiments were conducted with identical spatial and temporal resolution. The spatial resolution was $2 \times 2 \times 5 \text{ mm}^3$ and the temporal resolution was 3 s. For GRE-BOLD, $22 \times 22 \text{ cm}^2$ field-of-view (FOV) spirals with two interleaves were used with a 20-slice acquisition. For passband b-SSFP, the FOV was chosen to be $22 \times 22 \times 12 \text{ cm}^3$ covering the whole cerebral cortex (see Fig. 5a). The passband 3D b-SSFP acquisitions involved 14-interleave spirals and 24 k_z phase-encoding locations. The temporal resolution of the fMRI acquisition was 3 s with a T_R of 1.5 s for GRE-BOLD (two-shot spiral) and 8.928 ms for passband b-SSFP. For passband b-SSFP acquisitions, T_E was 1.632 ms and the readout duration per T_R was 3.392 ms. For the passband b-SSFP acquisitions, a 180° phase-cycling and a 0° phase-cycling acquisitions were combined with MIP as described in the two-acquisition method section.

The subjects were instructed to inhale and hold their breath when the screen showed a small red box in the middle of the visual field and to breathe normally when the box turned green. Breath-holding and normal breathing were alternated in 15-s intervals for 255 s starting and ending with a normal breathing period.

Full-Field Flashing Visual Checkerboard Experiment

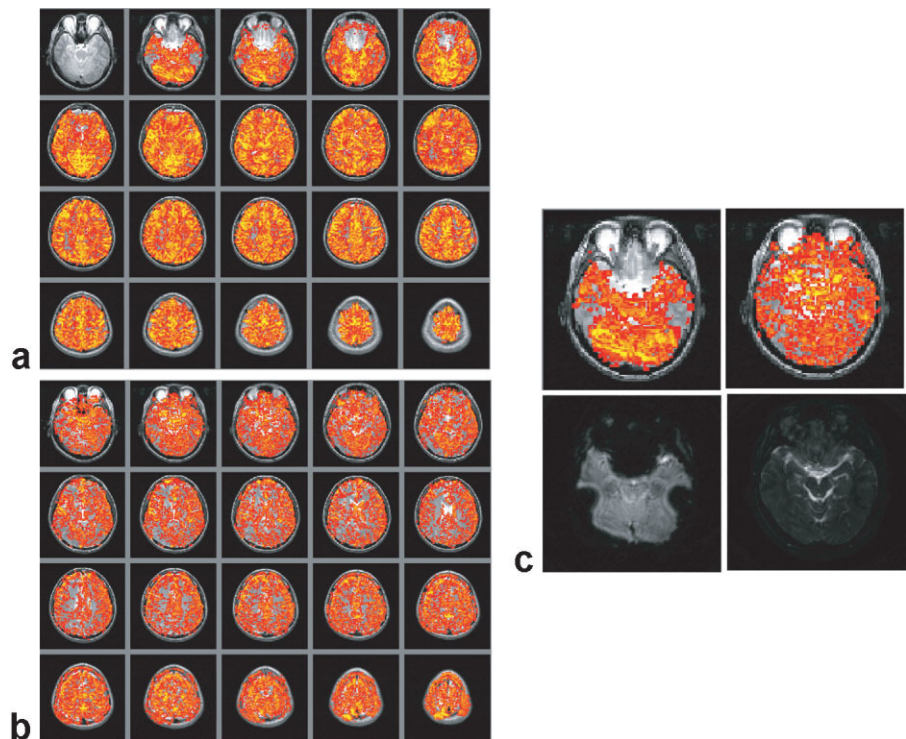
As an initial attempt to demonstrate the passband b-SSFP fMRI's capability to generate oxygenation contrast following stimulus-induced neuronal activation, simple on/off full visual-field flashing checkerboard experiments were performed. The flashing checkerboard on and off blocks were in 15-s intervals for a total duration of 2 min.

The resolution of the acquisition was $22 \times 22 \times 3 \text{ cm}^3$ and the resolution was $2 \times 2 \times 2 \text{ mm}^3$ to cover the visual cortex (see Fig. 5b). The 3D spiral acquisition consisted of 16 interleaved spirals and 16 k_z phase encodes. The temporal resolution was 2 s with a T_R of 8 ms and T_E of 2.104 ms. The readout duration was 3.344 ms per T_R . While a single acquisition was sufficient to cover the visual cortex, the two-acquisition scheme was chosen to demonstrate how distortion and signal-dropout free functional images can be obtained using two acquisitions.

Hemodynamic Response Function Measurement

For the comparison of the hemodynamic response functions (HRF) derived from passband and GRE-BOLD images, respectively, a full-visual field flashing checkerboard with a 3-s impulse duration was used. The impulse was repeated every 30 s for repeated measurements. The measurement was repeated six times every 30 s at each trial over two trials (12 measurements total). We averaged the signal across all voxels in the primary visual cortex (V1) (see Fig. 5c). V1 was identified using standard visual field mapping methodology (30,31) in previous scanning sessions with an identical stimulus setup. An oblique volume through the visual cortex was selected for both acquisitions. The passband b-SSFP acquisition FOV was $22 \times 22 \times 6 \text{ cm}^3$ and the spatial resolution was $2 \times 2 \times 3 \text{ mm}^3$. 3D spiral acquisitions used 14 interleaves with 12 phase-encoding locations in k_z , a T_R of 8.928 ms, T_E of 1.952 ms, and a readout duration of 3.392 ms per T_R . In order to show

FIG. 6. Hypercapnia experiment result. T_2 anatomical overlay of the activation pattern of the whole-brain breath-holding experiment using (a) GRE-BOLD and (b) Passband b-SSFP fMRI. c: A slice near the sinus off-resonance was selected for a zoomed view. The two activation maps on the top row and the two raw functional images on the second row are for GRE-BOLD and passband b-SSFP, respectively. Severe distortions and signal dropout for GRE-BOLD results in missing activation areas while the passband b-SSFP result shows no such effect.



the flip angle dependency in passband fMRI, the flip angle was varied from 20° to 70° in 10° steps. GRE-BOLD images were acquired with a 22-cm FOV and $3.4 \times 3.4 \times 5 \text{ mm}^3$ resolution. Temporal resolution was 1.5 s for both acquisitions.

Visual Field Mapping

High-resolution visual field mapping (30) was performed to demonstrate the high-resolution imaging capability of the passband b-SSFP fMRI. Visual field mapping was chosen since it produces extra temporal phase information that can be used to verify the passband b-SSFP fMRI techniques capability to accurately track the time course of the oxygenation signal. Visual field mapping experiments involved a stimulus with a contrast pattern comprising a rotating wedge (90°) that slowly rotated around fixation, completing a cycle in 42 s. The wedge rotated around six times (total duration 4 min 12 s).

Two different experiments were conducted for the high-resolution visual field mapping. For both experiments the FOV was $8 \times 8 \times 1 \text{ cm}^3$ covering the primary visual cortex. The temporal resolution was 3.5 s. One experiment had a spatial resolution of $1 \times 1 \times 1 \text{ mm}^3$ with a T_R of 10.936 ms and a T_E of 2.460 ms. The readout duration was 3.104 ms. The 3D spirals had 16 interleaves with 20 k_z phase encodes. The data were averaged from six runs. The other experiment had a spatial resolution of $0.9 \times 0.9 \times 0.9 \text{ mm}^3$ with a T_R of 11.364 ms and a T_E of 1.616 ms. The readout duration was 4.128 ms. The 3D spirals were designed to have 14 interleaves and 22 phase encoding in k_z . For this experiment the data were averaged from four runs.

Functional Data Analysis

The acquired 4D functional dataset was reconstructed with a gridding reconstruction (32). Using FSL (33), hy-

percapnia and the full field visual stimulation data were analyzed with a high-pass filter cutoff of 30 s, MCFLIRT motion correction, and BET brain extraction. Cluster thresholding was used with z threshold of 2.3 and cluster p threshold of 0.05. Custom software (VISTA, <http://white.stanford.edu/software>) was used for the hemodynamic response function measurements and the visual field map analysis. For the analysis using VISTA, no corrections other than high-pass filtering were used. For the hemodynamic response function measurements the primary visual cortex V1 was first identified. Then the signal was averaged over the selected region. The visual field map data was coherence thresholded (34) and overlaid onto T_1 or T_2 anatomical images and/or color coded on a flattened cortical surface. The coherence threshold was 0.3 for the 1 mm isotropic image acquisition and 0.5 for the 0.9 mm isotropic acquisition.

RESULTS

The experiments were all repeated across multiple-subjects but the results are presented in a single subject form to show the method's capability to produce robust, high-resolution activation maps in individual subject studies.

Breath-Holding Experiment

The breath-holding experiments, as shown in Fig. 6, demonstrate passband b-SSFP fMRIs capability to capture activations in the regions that are traditionally difficult to study using GRE-BOLD. The same axial slices covering the whole brain are displayed for GRE-BOLD (Fig. 6a) and passband b-SSFP (Fig. 6b), respectively. With GRE-BOLD, a large portion of the prefrontal cortex cannot be robustly imaged due to signal dropout. Passband b-SSFP, on the other hand, resulted in whole brain oxygenation contrast

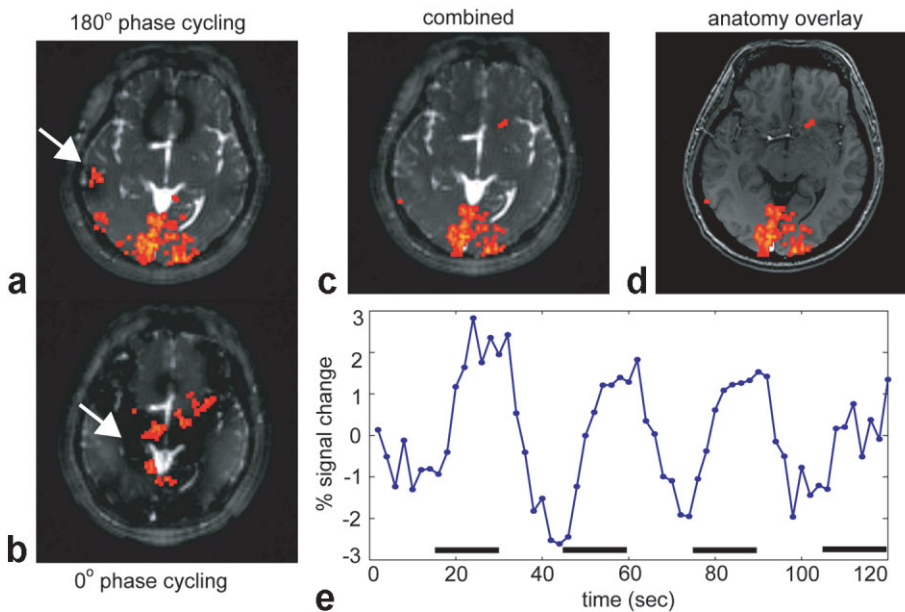


FIG. 7. Full visual field on/off experiment result. (a) 180° and (b) 0° phase-cycled b-SSFP acquisitions and corresponding activation maps. The individual images (a,b) show artifactual activations (white arrows) that occur in the banding areas where the signal exhibits strong frequency sensitivity. c: These artifactual activations can be eliminated by appropriately combining the two images. d: Due to the reduced distortion of b-SSFP acquisitions, high-quality anatomical registration can be done with simple translations. e: Signal average over all activated voxels. The horizontal bars indicate the stimulus-on period.

without marked spatial distortions or signal dropout, including in ventral-most prefrontal cortex. Panels in Fig. 6c demonstrate more clearly the differences in spatial distortions and coverage between the two techniques. The left two axial images display the GRE-BOLD results (top: thresholded activity map overlaid on T_2 anatomy; bottom: raw GRE-BOLD image) obtained from one of the ventral-most slices. Note the substantial signal dropout in prefrontal and ventrolateral areas. The corresponding passband b-SSFP images, on the other hand, (right two axial images in Fig. 6c), have no marked spatial distortions (bottom), and provide a homogenous oxygenation contrast throughout the brain (top) with potentially better localization in the gray matter region.

Full-Field Flashing Visual Checkerboard Experiment

Figure 7 depicts results from the full-visual-field stimulation experiments (see also Fig. 5b). Axial slices centered around the primary visual cortex are shown in this figure. Note that a single 180° phase-cycled acquisition (Fig. 7a) was sufficient to cover the primary visual cortices, as banding-related artifactual activities occurred only in localized regions outside of the visual cortex (marked by arrows in Fig. 7a,b). However, to demonstrate the applicability of the two-acquisition method (see Fig. 4), another set of data was acquired with a 0° phase-cycling angle (Fig. 7b). In both the 180° and the 0° acquisitions, false-positive activations were detected in the banding areas where the signal was unstable due to the rapid magnitude and phase transitions. After combination of the two phase-cycled images using MIP, most of the false activations were removed (Fig. 7c). Figure 7c also shows the lack of any noticeable spatial distortion for passband b-SSFP functional image. This becomes more evident when the passband b-SSFP image is compared with the corresponding anatomical image from the same subject (Fig. 7d): the outlines of the two brains closely match each other such that the passband b-SSFP functional image can be core-

gistered with the anatomical images with a simple translation (Fig. 7d). Figure 7e shows the signal average time course for all activated voxels from Fig. 7c.

Hemodynamic Response Function Measurement

Panels in Fig. 8 display the HRF computed from full visual field stimulation studies (see Fig. 5c). Figure 8a shows the HRF derived from GRE-BOLD signals. It shows the characteristic delayed oxygenation followed by signal reversal and undershoot (35). The resulting HRF for GRE-BOLD can be best described using two-gamma functions (36) (Fig. 8a). Before deriving the corresponding HRF from passband b-SSFP fMRI data, the question of optimum flip angle will have to be taken into consideration. While most imaging parameters such as T_E and T_R are constrained by other acquisition parameters such as scan time, imaging FOV, resolution, and readout time, the flip angle can be changed significantly without interfering with other imaging parameters. The flip angle is expected mainly to effect image contrast, as measured by HRF. Therefore, the optimal choice would be to use the flip angle that gives the maximum contrast. However, in b-SSFP another important criterion for flip angle selection is flat b-SSFP off-resonance profile (see Fig. 1c). In simulations (37), a flip angle of around 30° yields the flattest off-resonance profile (Fig. 8b). However, for our experimental measurement of HRF (Fig. 8c) we can assume the ROI for the full-field experiment to occupy only a narrow portion of the off-resonance profile; the measurement is then independent of the off-resonance profile's flatness. The measured HRF would therefore mostly represent the flip angle dependency of the contrast mechanism. Figure 8c demonstrates that the measured passband b-SSFP HRFs are not a very strong function of flip angles. This suggests that we can optimize the flip angle by focusing on maximizing the frequency width of the flat portion of the passband. Since no significant difference was observed in Fig. 8c, we were

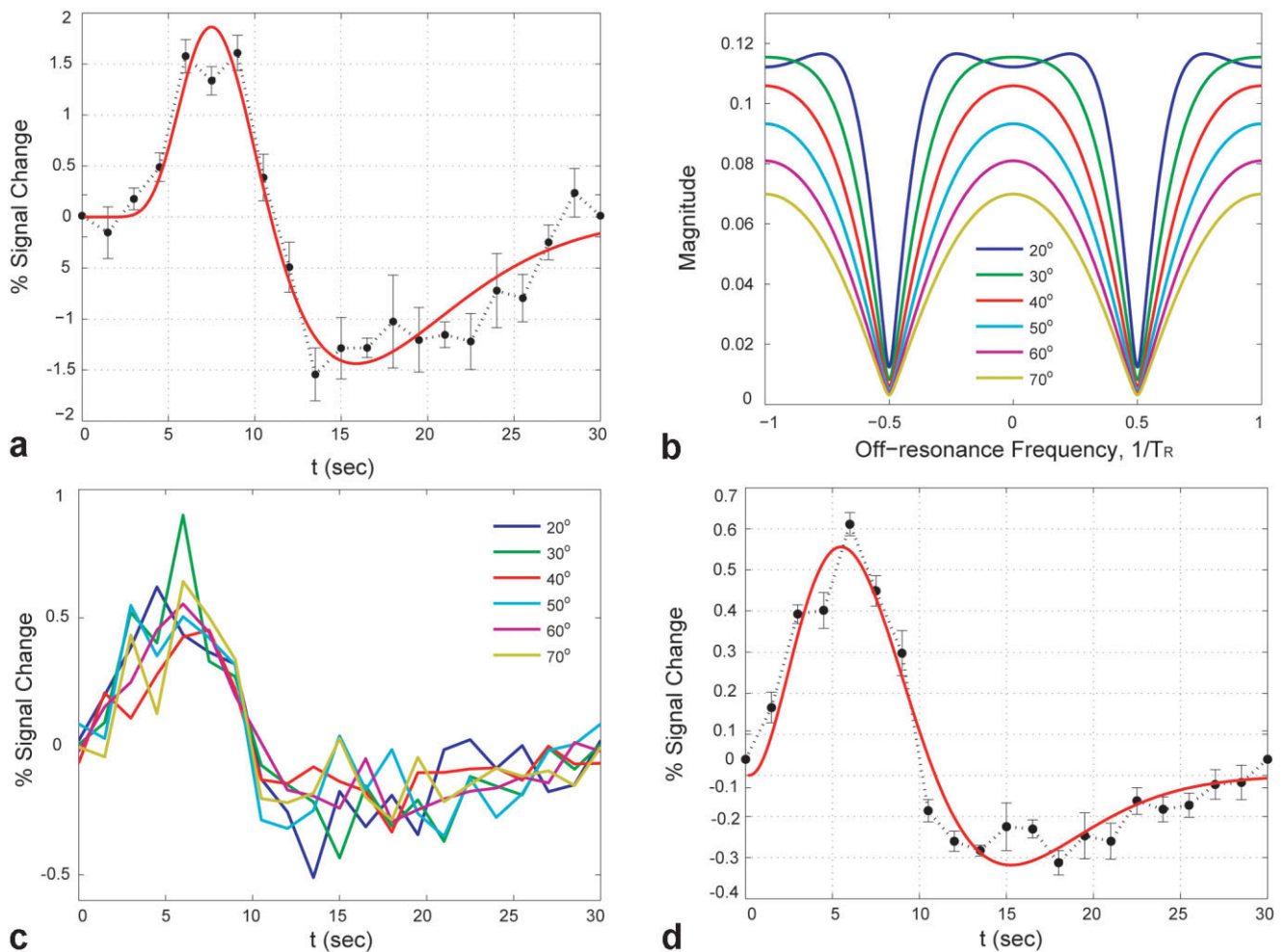


FIG. 8. **a:** GRE-BOLD hemodynamic response function matches a typical response. The two gamma function fit resulted in a T-value of 15.84, maximum amplitude of 1.86 at 7.5 s. Rise to half time was 5.4 s. **b:** Passband b-SSFP fMRI utilizes the flat portion of the b-SSFP off-resonance profile. Therefore, to obtain robust contrast over a large off-resonance region the flat portion has to be wide. The flip angle dependency of the off-resonance profile is plotted here for gray matter with T_1 , T_2 values at 3T ($T_1 = 1820$ ms, $T_2 = 99$ ms) obtained from a recent article (37). **c:** Passband b-SSFP hemodynamic response function was measured for flip angles ranging from 20–70°. However, the measured HRFs were not a very strong function of flip angles. **d:** Since no apparent difference was observed, to improve the SNR all six measurements were averaged and fitted with a two-gamma function. The two-gamma function t resulted in a T-value of 17.55, maximum amplitude of 0.56 at 5.55 sec. Rise to half time was 2.7 s.

able to collapse the six HRFs obtained for the six different flip angles into one average HRF. While the resulting HRF for passband b-SSFP fMRI (Fig. 8d) could accurately be fitted with two-gamma functions, the ascending portion of the passband b-SSFP's HRF was found to occur with smaller amplitude and shorter delay when compared to the GRE-BOLD HRF (compare Fig. 8a,d).

Visual Field Mapping

Figures 9 and 10 show the result of our visual field mapping studies (see Fig. 5d). Here, a 1-inch custom single loop surface coil positioned on top of the primary visual cortex was used for localized functional imaging. In Fig. 9a the phase of the coherence-thresholded activation maps were overlaid on the T_1 anatomical images (axial, sagittal, and coronal views, respectively) of the same spatial resolution (voxel size = 1 mm³). Note how the activated voxels tightly follow the

cortical gray matter, suggesting that they reflect predominantly neuronal activity. Furthermore, the panels in Fig. 9a demonstrate that passband b-SSFP retains adequate functional signals even at an isotropic 1 mm spatial resolution. Likewise, the thresholded activation map overlaid on an inflated brain (Fig. 9b) displays a typical visual field map representation of the brain obtained with our distortion-free passband b-SSFP functional data. The boundaries between V1 and V2 were identified using standard criteria.

The capability of passband b-SSFP for high spatial resolution functional imaging is further demonstrated in Fig. 10. Here, 900 μ m isotropic functional voxel resolution was achieved. Figure 10a displays a thresholded coherence map overlaid on a T_2 anatomical image of the same spatial resolution. Note how the activated voxels are tightly coned to the cortical gray matter. The time course obtained from an arbitrary selection of activated voxels from

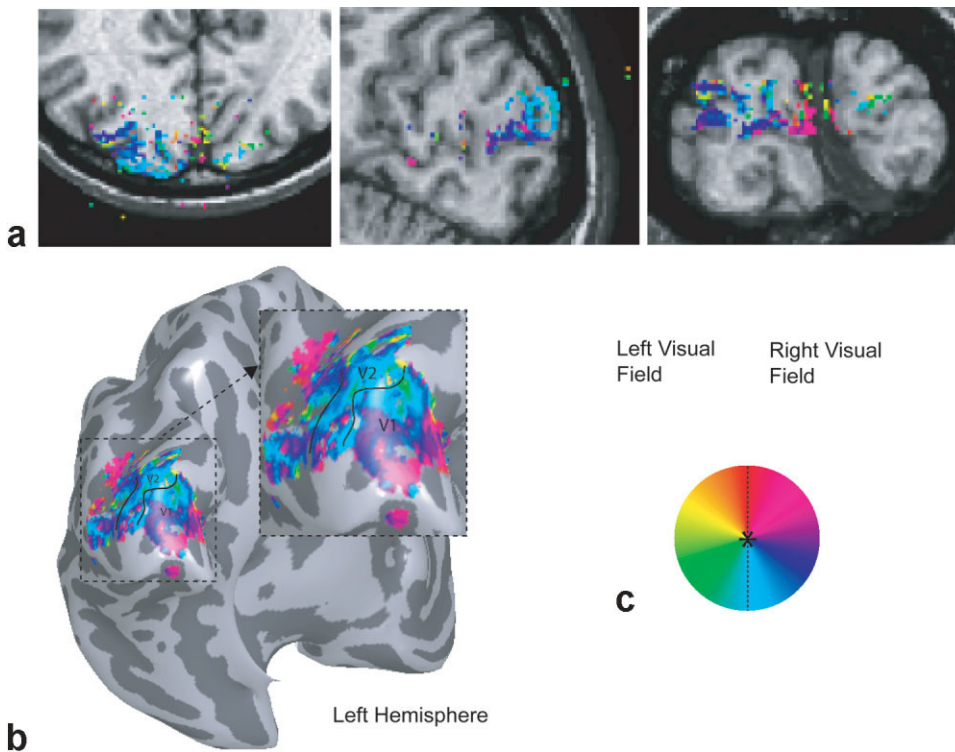


FIG. 9. Visual field mapping at isotropic 1 mm resolution. The phase of the thresholded voxels was overlaid on a T_1 anatomical image (a). The thresholded activation shows good correlation with the gray matter. The phase overlaid onto an inflated brain (b) shows the V1/V2 boundary. Color coding used for the visual field map is shown in (c).

Fig. 10a (see Fig. 10b) demonstrates the peak-to-peak reproducibility of activity even at this exceedingly high spatial resolution. Finally, the three time courses in Fig. 10c show a robust signal modulation even for voxels with less than a $0.73 \mu\text{L}$ volume.

DISCUSSION

In the present study we demonstrated several properties of passband b-SSFP-based functional imaging methods. The results of our studies suggest that passband b-SSFP

can provide distortion-free whole-brain coverage. Furthermore, with 3D acquisition schemes and small coils, isotropic submillimeter resolution functional data can be acquired within neuroscientifically relevant temporal resolution. We therefore conclude that distortion-free, whole-brain functional MRI and submillimeter resolution can now be performed using conventional MRI systems that are already available. However, significant research efforts will be required to gain a more complete understanding of the signal source and further optimization of the passband b-SSFP-based functional MRI methods.

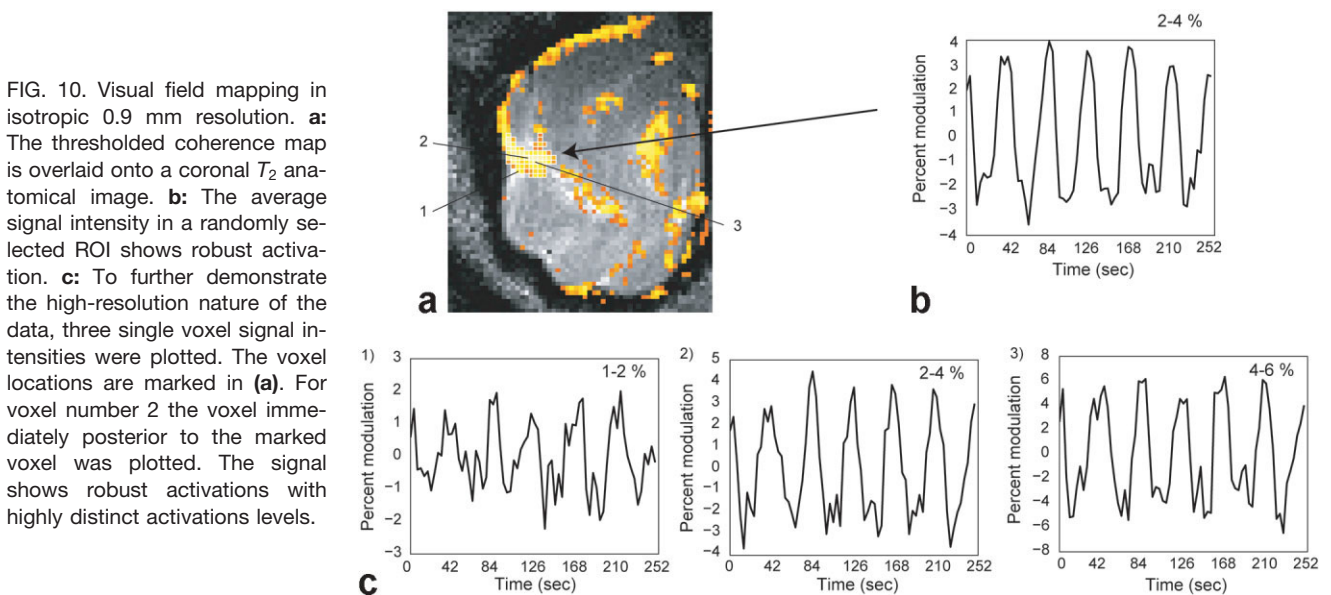


FIG. 10. Visual field mapping in isotropic 0.9 mm resolution. a: The thresholded coherence map is overlaid onto a coronal T_2 anatomical image. b: The average signal intensity in a randomly selected ROI shows robust activation. c: To further demonstrate the high-resolution nature of the data, three single voxel signal intensities were plotted. The voxel locations are marked in (a). For voxel number 2 the voxel immediately posterior to the marked voxel was plotted. The signal shows robust activations with highly distinct activations levels.

Contrast-to-Noise Ratio

Contrast-to-noise ratio (CNR) in passband b-SSFP fMRI is expected to be dependent on acquisition T_R , T_E , flip angle, and the spatial resolution at which the data was acquired. Parameters such as T_R , T_E , and flip angle has the potential to directly influence the contrast generation mechanism by which the CNR changes (12,15–18). However, when selecting the imaging parameters the significance of the effect has to be weighed against other constraints such as the flatness of the passband and SAR. The image resolution is also expected to impact CNR through changes in partial volume effects. At relatively low spatial resolutions (2–3 mm) and short T_R (<10 ms), the CNR of passband b-SSFP acquisitions generally seem smaller than that of GRE-BOLD acquisitions with faster response (see Fig. 8a,d), which is likely to be related to partial voluming effects and sensitivity to smaller vasculature rather than larger draining vessels. With submillimeter spatial resolution, however, small neighboring voxels start to show significantly different CNR. This is most likely due to the distinct vasculature within the neighboring voxels.

Scan Time and Coverage

Sufficient temporal resolution can be obtained for normal low-resolution large-volume coverage as well as high-resolution small-volume coverage using passband b-SSFP fMRI methods as demonstrated in Fig. 3 using fast 3D imaging trajectories. The added advantage of this technique, however, is that all the fast imaging techniques such as partial- k -space acquisitions (38), parallel imaging (39), and variable-density sampling (40) methods are compatible. These techniques can be combined to further improve the spatial and temporal resolution and volume coverage. Especially for high-resolution small-volume imaging, when combined with massive small coil arrays, whole-brain coverage will be achievable in high resolution.

As can be seen from Fig. 4, the MIP of two-acquisitions does not necessarily produce a flat magnitude response with two acquisitions. While two acquisitions will be sufficient for most applications as demonstrated, for applications where uniform spatial sensitivity is of great importance more phase-cycling angles can be acquired at the price of increasing scan time (28). Furthermore, as mentioned earlier, when whole-brain coverage is required with novel stimuli it is desirable to interleave the two phase-cycled passband b-SSFP acquisitions instead of repeating the two acquisitions. The interleaving, however, will decrease the temporal resolution due to the doubling of acquisition time for acquiring the two phase-cycling angles and the transition time between the two steady states.

While passband b-SSFP fMRI offers good spatial and temporal resolution (Fig. 3), 3D imaging is expected to give different temporal dynamics within each volume acquisition time. With the multi-slice approach used for GRE-BOLD, each slice is acquired separately over a shorter period of time compared to the total volume acquisition time. However, for 3D acquisitions the signal from the whole imaging volume is continuously acquired over the total volume-acquisition time. Therefore, even with the

sampling rate matched for GRE-BOLD and passband b-SSFP methods, the voxel signal capturing time is different. This will lead to different temporal dynamics which may or may not be significant.

REFERENCES

1. Carr H. Steady-state free precession in nuclear magnetic resonance. *Phys Rev Lett* 1958;112:1693–1701.
2. Oppelt A, Graumann R, Barfuss H, Fischer H, Hartl W, Shajor W. FISP — a new fast MRI sequence. *Electromedica* 1986;54:15–18.
3. Scheffler K, Seifritz E, Bilecen D, Venkatesan R, Hennig J, Deimling M, Haacke EM. Detection of BOLD changes by means of a frequency-sensitive trueFISP technique: preliminary results. *NMR Biomed* 2001; 14:490–496.
4. Miller KL, Hargreaves BA, Lee J, Ress D, deCharms RC, Pauly JM. Functional brain imaging using a blood oxygenation sensitive steady state. *Magn Reson Med* 2003;50:675–683.
5. Ogawa S, Lee TM, Nayak AS, Glynn P. Oxygenation-sensitive contrast in magnetic resonance image of rodent brain at high magnetic fields. *Magn Reson Med* 1990;14:68–78.
6. Ogawa S, Tank DW, Menon R, Ellermann JM, Kim SG, Merkle H, Ugurbil K. Intrinsic signal changes accompanying sensory stimulation: functional brain mapping with magnetic resonance imaging. *Proc Natl Acad Sci U S A* 1992;89:5951–5955.
7. Kwong KK, Belliveau JW, Chesler DA, Goldberg IE, Weisskoff RM, Poncelet BP, Kennedy DN, Hoppel BE, Cohen MS, Turner R. Dynamic magnetic resonance imaging of human brain activity during primary sensory stimulation. *Proc Natl Acad Sci U S A* 1992;89:5675–5679.
8. Miller KL, Smith SM, Jezzard P, Pauly JM. High-resolution FMRI at 1.5T using balanced SSFP. *Magn Reson Med* 2006;55:161–170.
9. Lee J, Dumoulin S, Glover G, Wandell B, Nishimura D, Pauly JM. Full-brain coverage and high-resolution imaging capabilities of passband SSFP fMRI at 3T. In: *Proc ISMRM, Berlin; 2007*. p 694.
10. Lee J, Gurney P, Dharmakumar R, Wright C, Hargreaves B, Shankaranarayanan A, Miller K, Nishimura D, Pauly J. Blood oxygenation (BOX) level dependent functional brain imaging using steady-state precession. In: *Proc ISMRM, Seattle; 2006*. p 3291.
11. Lee J, Gurney P, Dumoulin S, Wandell B, Shankaranarayanan A, Nishimura D, Pauly JM. BOX fMRI using multiple-acquisition steady-state free precession imaging for full-brain coverage. In: *Proc ISMRM, Seattle; 2006*. p 3297.
12. Zhong K, Leupold J, Hennig J, Speck O. Systematic investigation of balanced steady-state free precession for functional MRI in the human visual cortex at 3 Tesla. *Magn Reson Med* 2007;57:67–73.
13. Bowen C, Mason J, Menon R, Gati J. High field balanced-SSFP fMRI: examining a diffusion contrast mechanism using varied flip angles. In: *Proc ISMRM, Seattle; 2006*. p 665.
14. Bowen C, Menon R, Gati J. High end balanced-SSFP FMRI: a BOLD technique with excellent tissue sensitivity and superior large vessel suppression. In: *Proc ISMRM, Miami; 2005*. p 119.
15. Bieri O, Scheffler K. Effect of diffusion in inhomogeneous magnetic fields on balanced steady-state free precession. *NMR Biomed* 2007;20: 1–10.
16. Kim T, Lee J, Pauly JM. Analysis of the BOLD signal characteristics in balanced SSFP fMRI: a Monte-Carlo simulation. In: *Proc ISMRM, Berlin; 2007*. p 696.
17. Miller KL, Smith SM, Jezzard P, Wiggins GC, Wiggins CJ. Signal and noise characteristics of SSFP fMRI: a comparison with GRE at multiple field strengths. *Neuroimage* 2007;37:1227–1236.
18. Klarhöfer M, Bieri O, Scheffler K. Diffusion effects in passband balanced SSFP fMRI. In: *Proc ISMRM, Berlin; 2007*. p 1641.
19. Dharmakumar R, Hong J, Brittain JH, Plewes DB, Wright GA. Oxygen-sensitive contrast in blood for steady-state free precession imaging. *Magn Reson Med* 2005;53:574–583.
20. Dharmakumar R, Qi X, Hong J, Wright GA. Detecting microcirculatory changes in blood oxygen state with steady-state free precession imaging. *Magn Reson Med* 2006;55:1372–1380.
21. Le Bihan D, Urayama S, Aso T, Hanakawa T, Fukuyama H. Direct and fast detection of neuronal activation in the human brain with diffusion MRI. *Proc Natl Acad Sci U S A* 2006;103:8263–8268.
22. Moore CI, Stern CE, Corkin S, Fischl B, Gray AC, Rosen BR, Dale AM. Segregation of somatosensory activation in the human rolandic cortex using fMRI. *J Neurophysiol* 2000;84:558–569.

23. Ugurbil K, Toth L, Kim DS. How accurate is magnetic resonance imaging of brain function? *Trends Neurosci* 2003;26:108–114.
24. Constable RT, Spencer DD. Composite image formation in z-shimmed functional MR imaging. *Magn Reson Med* 1999;42:110–117.
25. Glover GH, Thomason ME. Improved combination of spiral-in/out images for BOLD fMRI. *Magn Reson Med* 2004;51:863–868.
26. Jezzard P, Clare S. Sources of distortion in functional MRI data. *Hum Brain Mapp* 1999;8:80–85.
27. Studholme C, Constable RT, Duncan JS. Accurate alignment of functional EPI data to anatomical MRI using a physics-based distortion model. *IEEE Trans Med Imaging* 2000;19:1115–1127.
28. Bangerter NK, Hargreaves BA, Vasanaawala SS, Pauly JM, Gold GE, Nishimura DG. Analysis of multiple-acquisition SSFP. *Magn Reson Med* 2004;51:1038–1047.
29. Kastrup A, Li TQ, Takahashi A, Glover GH, Moseley ME. Functional magnetic resonance imaging of regional cerebral blood oxygenation changes during breath holding. *Stroke* 1998;29:2641–2645.
30. Engel SA, Glover GH, Wandell BA. Retinotopic organization in human visual cortex and the spatial precision of functional MRI. *Cereb Cortex* 1997;7:181–192.
31. Sereno MI, Dale AM, Reppas JB, Kwong KK, Belliveau JW, Brady TJ, Rosen BR, Tootell RB. Borders of multiple visual areas in humans revealed by functional magnetic resonance imaging. *Science* 1995;268:889–893.
32. Jackson J, Meyer C, Nishimura DG, Macovski A. Selection of a convolution function for Fourier inversion using gridding. *IEEE Trans Med Imaging* 1991;10:473–478.
33. Smith SM, Jenkinson M, Woolrich MW, Beckmann CF, Behrens TE, Johansen-Berg H, Bannister PR, De Luca M, Drobnjak I, Flitney DE, Niazy RK, Saunders J, Vickers J, Zhang Y, De Stefano N, Brady JM, Matthews PM. Advances in functional and structural MR image analysis and implementation as FSL. *Neuroimage* 2004;23(suppl 1):S208–219.
34. Bandettini PA, Jesmanowicz A, Wong EC, Hyde JS. Processing strategies for time-course data sets in functional MRI of the human brain. *Magn Reson Med* 1993;30:161–173.
35. Buxton RB, Wong EC, Frank LR. Dynamics of blood flow and oxygenation changes during brain activation: the balloon model. *Magn Reson Med* 1998;39:855–864.
36. Glover GH. Deconvolution of impulse response in event-related BOLD fMRI. *Neuroimage* 1999;9:416–429.
37. Stanisz GJ, Odobina EE, Pun J, Escaravage M, Graham SJ, Bronskill MJ, Henkelman RM. T_1 , T_2 relaxation and magnetization transfer in tissue at 3T. *Magn Reson Med* 2005;54:507–512.
38. Lee J, Pauly JM, Nishimura DG. Partial k-space reconstruction for under-sampled variable-density spiral trajectories. In: *Proc ISMRM, Toronto*; 2004. p 475.
39. Pruessmann KP, Weiger M, Bornert P, Boesiger P. Advances in sensitivity encoding with arbitrary k-space trajectories. *Magn Reson Med* 2001;46:638–651.
40. Lee JH, Hargreaves BA, Hu BS, Nishimura DG. Fast 3D imaging using variable-density spiral trajectories with applications to limb perfusion. *Magn Reson Med* 2003;50:1276–1285.